

## CHEMICAL PHYSICS

# Augmenting the living plant mesophyll into a photonic capacitor

Pavlo Gordiichuk<sup>1</sup>, Sarah Coleman<sup>1,2</sup>, Ge Zhang<sup>1</sup>, Matthias Kuehne<sup>1</sup>, Tedrick T. S. Lew<sup>1,3</sup>, Minkyung Park<sup>1</sup>, Jianqiao Cui<sup>1</sup>, Allan M. Brooks<sup>1</sup>, Karaghen Hudson<sup>4</sup>, Anne M. Graziano<sup>4</sup>, Daniel J. M. Marshall<sup>4</sup>, Zain Karsan<sup>4</sup>, Sheila Kennedy<sup>4</sup>, Michael S. Strano<sup>1\*</sup>

Living plants provide an opportunity to rethink the design and fabrication of devices ordinarily produced from plastic and circuit boards and ultimately disposed of as waste. The spongy mesophyll is a high-surface area composition of parenchyma cells that supports gas and liquid exchange through stomata pores within the surface of most leaves. Here, we investigate the mesophyll of living plants as biocompatible substrates for the photonic display of thin nanophosphorescent films for photonic applications. Size-sorted, silica-coated  $650 \pm 290$ -nm strontium aluminate nanoparticles are infused into five diverse plant species with conformal display of 2- $\mu\text{m}$  films on the mesophyll enabling photoemission of up to  $4.8 \times 10^{13}$  photons/second. Chlorophyll measurements over 9 days and functional testing over 2 weeks at 2016 excitation/emission cycles confirm biocompatibility. This work establishes methods to transform living plants into photonic substrates for applications in plant-based reflectance devices, signaling, and the augmentation of plant-based lighting.

## INTRODUCTION

There has been substantial interest in using living plants to create functional devices that replace those fabricated from plastic and circuit boards, and are ultimately disposed of as waste (1–10). Examples of these devices include the use of plant leaves as sensors for the detection of plant mechanical wounding (11), development of biocompatible plant-based electronic semiconductors and electrochromic pixels (4), and plant adenosine triphosphate (ATP)-powered genetically encoded autoluminescent light sources (6–8) as sustainable alternatives. The plant leaf itself, in particular, has specific optical properties that enable its functions of photosynthesis and reflectance (12). However, to date, there has not been a study on how to change these properties in plants to achieve additional functions, such as phosphorescence, in pursuit of these larger sustainability goals. The hypothesis addressed in this work is whether the plant spongy mesophyll itself can provide a photonic substrate to enhance or augment plant-based photonics and light emission specifically. This is a scientific question because the biocompatibility, particle adhesion, and mesophyll hydraulic function upon nanoparticle (NP) deposition are not known. In this work, we investigate how NPs can be infiltrated into the leaf mesophyll (Fig. 1A) to change its ability to absorb, store, and re-emit incident light. The resulting photonic capacitance will help to introduce functional optics into living plants with the particular localization in the plant mesophyll area, fully biocompatible and functional.

There have been significant advances toward the conversion of living plants into functional devices; however, photonic modifications have not been studied to date, particularly with NP approaches (9). For example, Giacomo *et al.* (3) applied plant cells and carbon

nanotube composites to develop state-of-the-art electronic temperature sensors. We previously used a DNA-wrapped carbon nanotube to transform living spinach plants into ground-water monitoring sensors and described methods for the modification of plant optical properties (2). Stavrinidou *et al.* (4) synthesized conducting organic polymers inside plants, with the potential for creating electrical conductors in living plants. As a distinct objective, we used NP techniques to transform living watercress plants into chemiluminescent lamps that emit light at an average intensity of  $10^{10}$  photons/s (5). However, these past techniques do not address or change the optical properties of the leaf itself. Others have genetically modified plants to emit light using bioluminescence genes (8), the six genes of the lux operon (7), or the firefly enzyme Luciferase (6). However, no work to date has focused on manipulating the optical properties of the leaves themselves, and their control in terms of absorption, light storage, and re-emission. This is despite the obvious benefits of such control to the overall aim of creating living plant light sources and optical sensors.

In addition to studies that functionalize plants, researchers have also explored the interface of materials with living plants, however, not the underlying spongy mesophyll, for other applications. Nassar *et al.* (13) applied wearable electronic circuits to plant leaves to monitor microclimate and growth conditions. Similarly, Zhao *et al.* (14) developed stretchable sensors for long-term studies on plant leaves. Tang *et al.* (15) developed a chitosan-based ink for plant growth monitoring with the flexible sensor. We applied microfluidic-printed stomata sensors allowing the continual monitoring of drought conditions in plants (16). Last, Damak *et al.* (17) developed a strategy for enhancing water deposition on plant leaves via an in situ precipitation strategy that used charged polymers sprayed from two nozzles.

While these external devices are useful, the application of nanomaterials inside plant leaves confers several alternate advantages. These nanomaterials can serve the role of a real-time reporter, monitoring analytes taken up by roots (2) [such as nitric oxide (9)], probing the innate plant signaling pathways in response to external stresses (11), or serving as an organelle-specific nanocarrier for genetic

Copyright © 2021  
The Authors, some  
rights reserved;  
exclusive licensee  
American Association  
for the Advancement  
of Science. No claim to  
original U.S. Government  
Works. Distributed  
under a Creative  
Commons Attribution  
NonCommercial  
License 4.0 (CC BY-NC).

<sup>1</sup>Department of Chemical Engineering, Massachusetts Institute of Technology, Cambridge, MA 02141, USA. <sup>2</sup>Department of Chemical Engineering, University of Texas at Austin, Austin, TX 78712, USA. <sup>3</sup>Institute of Materials Research and Engineering, Agency for Science, Technology and Research (A\*STAR), Singapore 138634, Singapore. <sup>4</sup>Department of Architecture, Massachusetts Institute of Technology, Cambridge, MA 02141, USA.

\*Corresponding author. Email: strano@mit.edu

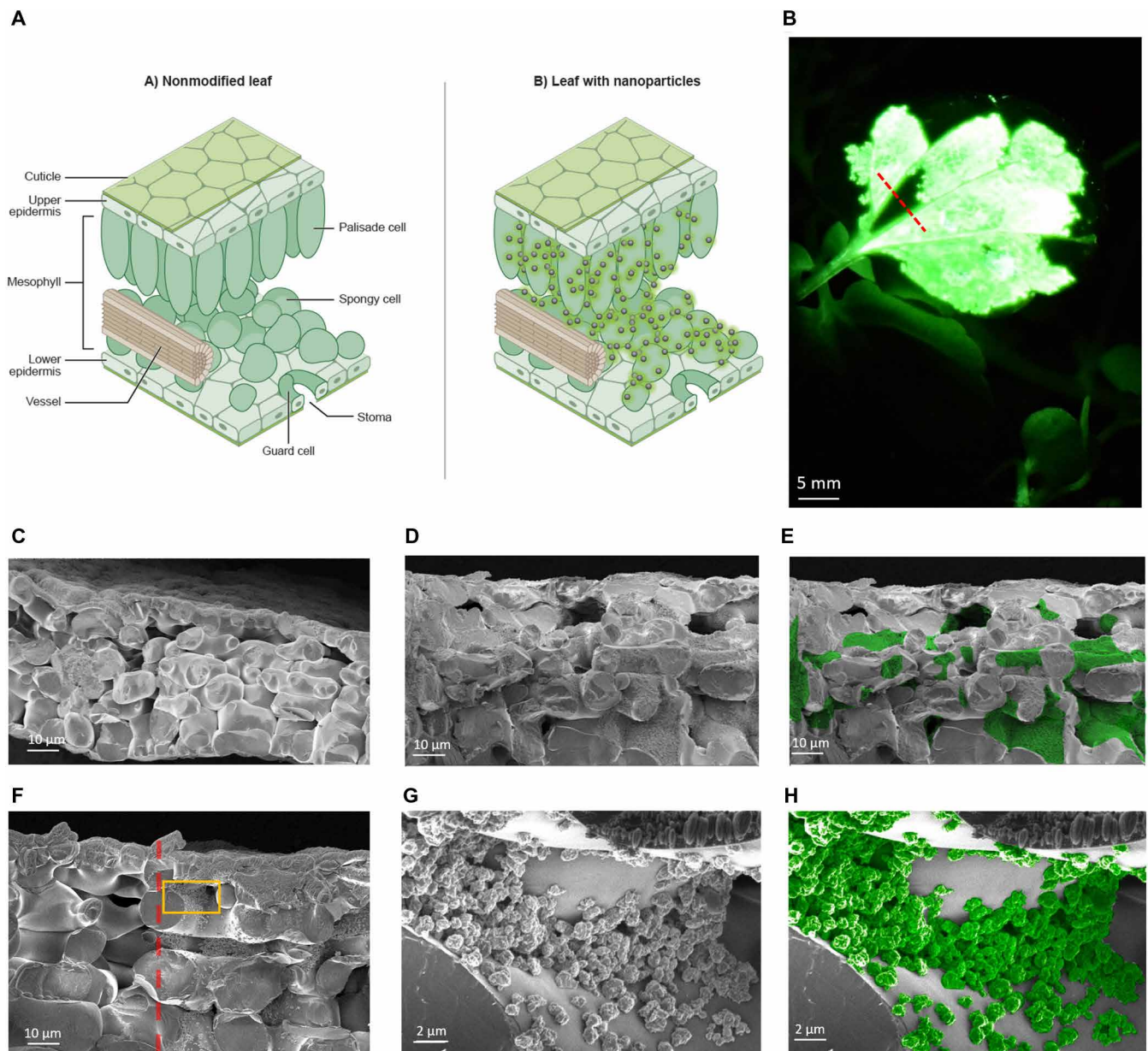


**Fig. 1. SA NP infiltrated in living plants.** (A) (Left) Schematic image of the mesophyll region of a plant leaf. The image shows cuticle, upper epidermis, mesophyll region, lower epidermis, vessel, palisade cells, spongy cells, guard cells, and stomata. (Right) Schematic image of the modified leaf with the SA NPs. (B) Light emission (after charging for 10 s with  $400 \text{ mW/cm}^2$  400-nm light source) infused in 3-week-old watercress leaf with solution of  $650 \pm 290 \text{ nm}$  SA NP (25 mg/ml). The image was captured on camera set on 30-s exposure time. (C) Cryo-SEM image of nonmodified freeze-fractured watercress leaf. Scale bar,  $10 \mu\text{m}$ . (D and E) Original and false-colored cryo-SEM images of freeze-fractured modified watercress leaf with solution of  $650 \pm 290 \text{ nm}$  SA NPs (25 mg/ml). Scale bar,  $2 \mu\text{m}$ . (F) Cryo-SEM images of freeze-fractured partially infiltrated watercress leaf [the direction of the fracture is shown with the red line in (B)] having both nonmodified (left side) and modified (right side) with  $650 \pm 290\text{-nm}$  SA NP NP regions. Orange box shows the zoom region for the next images. Scale bar,  $10 \mu\text{m}$ . (G and H) Original and false-colored zoom of the cryo-SEM images of SA-modified region in watercress leaf with solution of  $650 \pm 290 \text{ nm}$  SA NP. Scale bar,  $2 \mu\text{m}$ . Photo credit: Pavlo Gordiichuk, Massachusetts Institute of Technology.

engineering in plants (18–20). The passive transport of NPs into plant protoplasts can be controlled by tuning their size and charge, established by a theoretical model called lipid exchange envelope penetration developed by our group (LEEP) (21). Despite this progress in understanding NP transport and localization in plant cells, there has not been a study addressing how NPs can interact with the mesophyll of the plant to modify its optical properties.

In contrast to previous reports leading to the development of light-emitting plants via nanobionics (5) and genetic modification strategies (6–8), we aim for decoration of plant mesophyll surfaces with photoactive materials having photoemission properties upon multiple excitations without the application of chemical reactions or infusions. In this work, we show that several plants such as tobacco (*Nicotiana tabacum*), basil (*Ocimum basilicum*), daisy (*Bellis perennis*),

watercress (*Nasturtium officinale*), and elephant ear (*Colocasia*) can be converted into a plant-based photonic device by stomata infusion using an optimal size of  $650 \pm 290$  nm strontium aluminate (SA) NPs. We show that using SA particles with weak interparticle potentials, homogeneous and high-density coverage of the mesophyll can be obtained *in vivo*. We demonstrate that there is a characteristic difference in performance between NPs infused in different plant types, an indication that the mesophyll surface area plays a crucial role in the morphology and resulting photo-optical properties. We examine the biocompatibility in the form of chlorophyll concentrations [soil plant analysis development (SPAD)] across watercress plants and measure phosphorescent decay times as a function of particle properties. Our work establishes the fabrication and characterization methods required to transform living plants into functioning photonic substrates with useful phosphorescent capacitance, creating opportunities for plant-based optical reflectance, signaling, and light emission.

## RESULTS

The central question asked in this work is whether the plant spongy mesophyll itself can provide a photonic substrate to enhance or augment plant-based photonics and light specifically. The overall strategy of plant modification explored in this work is to infiltrate the mesophyll of the plant leaf through the surface stomata pores, dispersing the particles onto the three-dimensional (3D) surface area of the spongy tissue (Fig. 1A). In this work, we focus on phosphorescent NPs with the goal of modifying the absorption, photonic storage, and phosphorescent emission of the living plant leaf. Once dispersed within the leaf tissue, we can assess optical properties of the NP layer, including phosphorescent lifetime, spatial imaging, characterization, and quantum yield. Figure 1B shows a typical phosphorescent emission of partially infused watercress leaf with the phosphorescent NP. Our study on the modified leaf with cryo-scanning electron microscopy (cryo-SEM) showed that the initial structure of the leaf (Fig. 1C) remains intact even after infusion of the particle solution with a concentration of up to 25 mg/ml (Fig. 1, D and E). In addition, observed particle aggregations and their permanent localization *in vivo* result from specific interparticle and particle-cell interactions happening inside the plant, which may change the optical properties by plant structure. The analysis of the boundary region of the nonmodified and modified areas of the same watercress leaf (Fig. 1F) showed the intact mesophyll cells in both cases. In addition, the detailed imaging (Fig. 1, G and H) showed the dispersed NP phase on the 3D spongy mesophyll on a section of a watercress leaf with the sharp boundary of the infiltrated region. In this work, we ask what are the optimal particle sizes and surface chemistry to enable infiltration and biocompatibility and long-term stability of the optical properties. The experiments below map out the trade-off between phosphorescent particle size and decay time.

We chose SA ( $\text{SrAl}_2\text{O}_4:\text{Eu}^{2+}, \text{Dy}^{3+}$ ) as a model photonic material for this study because of its prior applications in illumination (22), numerical and graphical displays (23), light-emitting diodes (LEDs) (24, 25), and glowing polymer composites (26, 27). We also note that phosphors like this could enhance plant-based lighting by storing and re-emitting incident or internally generated light. We adapted a wet-milling method (28, 29) followed by centrifugation to size-select ranges of SA particle diameters. Initially, SA powder with particle sizes ranging from 3 to 5  $\mu\text{m}$  was wet-milled for 1 week and coated

with a Si/SiO<sub>2</sub> shell (mSA). This modification allowed particle stabilization in solution, which enabled further particle sorting by centrifugation (see the “Part 1” section in Materials and Methods). We first sought to optimize SA particle diameter for the desired optical properties while maintaining biocompatibility and the ability to be infused into the plant.

To address this, we centrifugally sorted SA particles at times ranging from 1 to 10 min, resulting in size-sorted ranges between 380 and 180 nm (Fig. 2, A and B). We found a direct relationship between milled SA diameter and phosphorescent decay time from  $1.8 \pm 0.3$  min for the largest particle to  $0.3 \pm 0.01$  min for the smallest particle. This is consistent with surface defects formed during the milling process, which introduce irradiative decay pathways into the otherwise stable light capacitance of the phosphor. However, these defects may form independently of the synthesis procedure, because we also replicated a micro-emulsion method (30) followed by thermal treatment at 1100°C, yielding much smaller NPs with an average size of  $11 \pm 1.0$  nm (fig. S1) and measured emission half-life of  $30 \pm 10$  s. Other literature reports find a decrease in phosphorescent lifetime with size in solid-phase particle samples (no solvent) from other preparation strategies, also attributed to defects (31–34). For photonic applications, this irradiative suppression of the light capacity should be minimized, forming the first constraint and trade-off for plant modification. Commercial microscopic SA powders prepared using a solid-state synthetic approach can show phosphorescence for up to 8 hours (5), but diameters above 1  $\mu\text{m}$  are impossible to infuse within the plant stomata, which range from 10 to 15  $\mu\text{m}$  in size with an opening gap less than 1  $\mu\text{m}$  across (cryo-SEM images in fig. S2).

While these samples had a minor increase in decay times compared to the previous strategy, they were still lower than dry powder ( $\tau = 20 \pm 0.5$  min; fig. S3). Therefore, we explored larger particle sizes (Fig. 2, D to F). We used a modified particle sorting strategy (see the “Part 2” section in Materials and Methods) to extract larger Si-coated mSA particles (Fig. 2A). We characterized all these samples by SEM (fig. S4), resulting in size distributions of  $390 \pm 180$ ,  $440 \pm 270$ ,  $650 \pm 290$ ,  $900 \pm 360$ , and  $1100 \pm 400$  nm, respectively (Fig. 2, D to F). Similar to our previous experiment, the particles (named S<sub>1</sub> to S<sub>5</sub>) collected in the water had decay times of 2.6, 3.1, 3.6, 3.6, and  $3.7 \pm 0.1$  min, respectively. The observed size-dependent decay times may be explained by possible defects present at the particle surface introduced from the milling step. We explain the defect-driven, size-dependent decay times with a theoretical model that we developed for our entire range of particle samples (Fig. 2C). This model describes the size-dependent irradiative decay (Supplementary Materials) trend in Fig. 2C consistently as a function of the defective surface thickness ( $\sim 26$  nm,  $\delta$ ), bulk (nonmilled) half-time (4.6 min,  $\tau_1$ ), and surface half-time (0.13 min,  $\tau_2$ ). However, decay is also a function of particle concentration, as we describe below.

The Si/SiO<sub>2</sub> coating significantly improves the plant biocompatibility of the SA. Wet-milled, uncoated SA particles, when dissolved in an aqueous solution, increase solution pH from 7 to as high as 14. We found that applying the Si/SiO<sub>2</sub> protecting shell prevents this. We must take sufficient care to prevent degradation of the Si/SiO<sub>2</sub> coating inside the plant mesophyll to maintain biocompatibility. To study the *in vivo* longevity of our Si/SiO<sub>2</sub>-coated particles, we infiltrated each NP type, coated or uncoated, and at various pH values, into 3-week-old watercress plants (*N. officinale*) to assess biocompatibility. We measured chlorophyll concentration in infiltrated and non-infiltrated leaves over 10 days (35) with a handheld SPAD-502 meter,

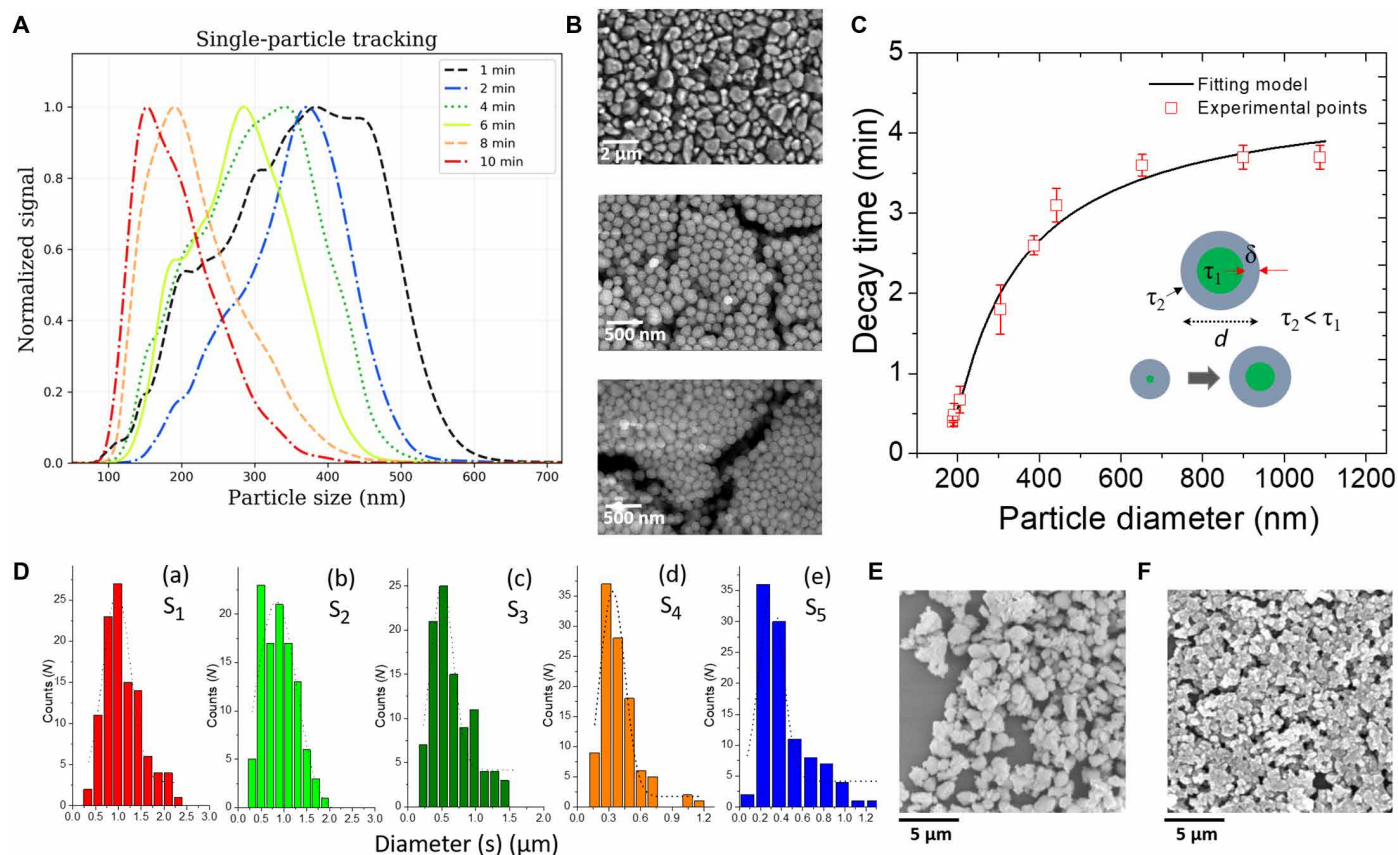


**Fig. 2. SA NP sorting and size-dependent decay time analysis.** (A) Plot showing size distributions measured in six samples of SA NPs collected between 1 and 10 min of centrifuging times measured with NanoSight single-particle tracking technique. (B) Selected typical SEM images of SA samples collected at 1-min (top), 6-min (middle), and 10-min (bottom) centrifuging steps. (C) Experimental SA NP decay time fit with the surface defect model (Supplementary Materials, model 1) upon the increase in NP size. (D) Histograms (A to E) of SA samples collected at different rpm speeds ranging from 0.5 to 4 K (presented as  $S_1$  to  $S_5$ ). (E and F) SEM image of the sample collected at 500 rpm ( $S_1$ ) and 4000 rpm ( $S_5$ ), respectively ( $S_1$  and  $S_5$ ). Scale bar, 5  $\mu\text{m}$ .

which gives an accurate and nondestructive measurement of leaf chlorophyll concentrations. Several parameters such as SA particle size, the presence of a Si/SiO<sub>2</sub> protective shell, pH, and particle concentration ranging from 1 to 50 mg/ml were studied (Fig. 3, A to C). To our knowledge, we have collected the most extensive dataset of photonic NP biocompatibility in the literature, with SPAD data averaged over 150 modified plants with SA/Si/SiO<sub>2</sub> compared to 30 control plants over 10 days.

We observed that the measured chlorophyll concentrations of the unmodified plants decreased by about 15% over 10 days, typical of plant maturation and internal growth regulation mechanisms associated with fast-growing plants (36). The infiltrated pristine SA (Fig. 3D) and pristine Si-coated SA particles (Fig. 3H) compromised the life span of infiltrated leaves, as reflected by the sharp decrease in chlorophyll level. We note that larger particles (>600 nm) required multiple infiltration points because of the difficulty of infiltration, which resulted in some mechanical damage and chlorophyll reduction in plant leaves (~45%). These large particles might further engage in stomata blocking events. We can resolve the complexity of this infiltration with smaller-size, milled samples; because the pore size of stomata is only about 1 to 2  $\mu\text{m}$  across, larger particles may not pass through, reducing cellular respiration in plants.

Last, the milled SA particles at pH 14 showed a drastic reduction of chlorophyll at all applied concentrations (~50%), showing the importance of maintaining the Si/SiO<sub>2</sub> coating of particles within the mesophyll to avoid plant toxicity (Fig. 3E). For example, we applied the same samples, neutralized to pH 7 with acetic acid (Fig. 3F) or after 3 weeks of dialysis (Fig. 3G), and observed only a minor reduction of chlorophyll concentration (~15%), approximately consistent with unmodified plants. In contrast, Si-coated mSA particles showed efficient particle infiltration into leaves and along with the leaves without damaging them (Fig. 3I). Particle concentrations of 1, 5, and 10 mg/ml exhibited no visible change, whereas highly concentrated samples showed a small (~5%) reduction in chlorophyll concentration compared to the nonmodified plants. Last, 20 watercress leaves infiltrated with mSA (50 mg/ml) were imaged optically directly after infiltration, and 1 week later, fig. S5 and this comparison showed no changes.

Confocal microscopy images (Fig. 4) show that our infiltration strategy resulted in homogeneous particle distribution inside the watercress leaf. Phosphor particles are located between cells and do not enter the mesophyll in modified leaves (Fig. 4, C and F). This observation supports our previously developed LEEP theory of NP transport within plant cell systems because the particles'  $\zeta$  potential

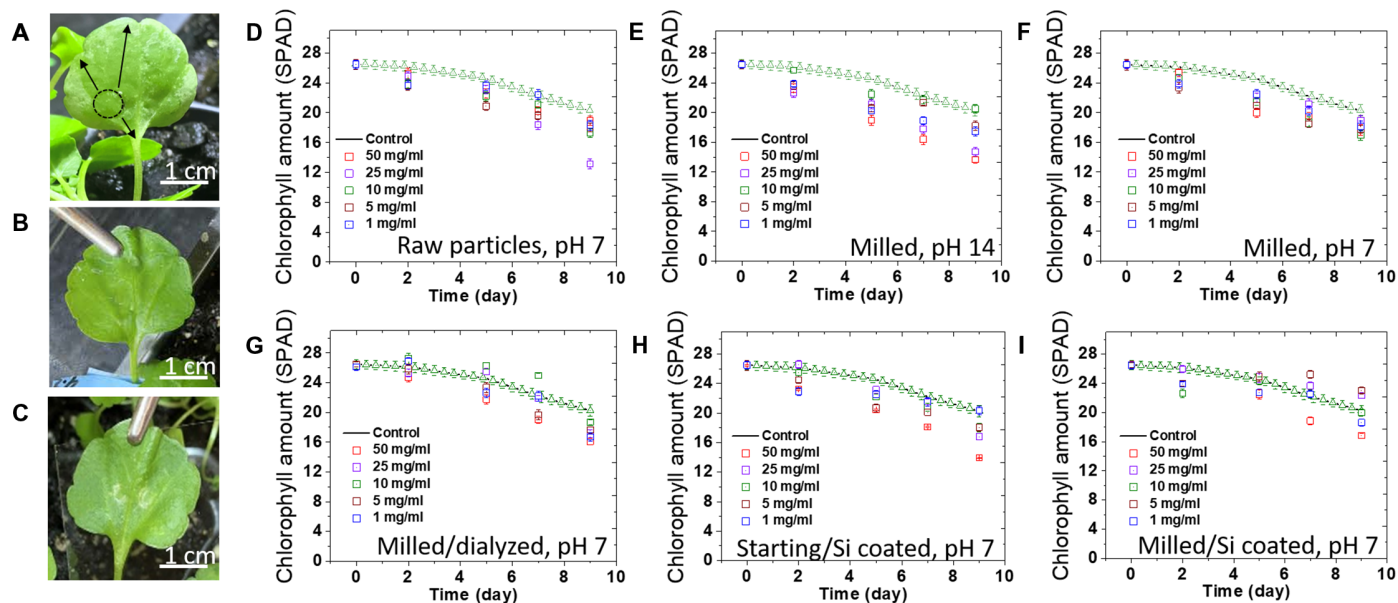


**Fig. 3. The biocompatibility of SA NP infusion into the plant mesophyll.** Influence of particle physical conditions such as size, Si/SiO<sub>2</sub> coating, and pH level of infiltrated solutions on the physiological properties of modified plants. (A) Fully infiltrated watercress leaf and plant with an indicated infiltrated point. (B) Optical image of 3-week-old watercress leaves directly after infiltration. (C) Optical image of the same modified watercress leaves after 12 days. Chlorophyll concentration measurements (in SPAD units) of infiltrated watercress leaves where (D) raw SA material showed lower chlorophyll concentration in modified plants, (E) milled SA (mSA) material at pH 14 led to much less chlorophyll, (F) mSA at pH 7 caused the minor effect to the modified plants, (G) mSA dialyzed at pH 7 showed a minor decrease in chlorophyll, (H) raw (~2 to 3  $\mu\text{m}$ ) material coated with Si/SiO<sub>2</sub> showed large reduction in chlorophyll, and (I) mSA coated with Si/SiO<sub>2</sub> at pH 7 showed the minimum impact on chlorophyll concentration. All samples were studied at concentrations of 1, 5, 10, 25, and 50 mg/ml, over 5 plants, resulting in 150 studied modified plants and 30 nonmodified intact plants. Photo credit: Sarah Coleman, Massachusetts Institute of Technology (S.C.).

(both  $+28.7 \pm 1.7$  mV for noncoated and  $-46.4 \pm 4.6$  mV for Si/SiO<sub>2</sub>-coated) and sizes are below the threshold required for passive penetration into the plant cells (21). We conducted further studies on leaf tissue integrity with cryo-SEM, which revealed that NPs in the infiltrated watercress leaf were located in the spongy mesophyll regions (Fig. 1, E and F). Detailed images show that particles homogeneously occupy open cavities inside the plant leaf in the lower epidermis region but only on the same side as the infiltration (Fig. 1, C and D). This supports the central question addressed in this work of whether it is possible to use the living plant mesophyll as a photonic substrate. The watercress leaf infiltrated with buffer showed no particles inside but a similar mesophyll structure. This demonstrates the nondamaging effect of infiltration on leaf internal structure. The non-infiltrated leaf revealed the smooth structure of the mesophyll, characteristic of a leaf of a pristine plant (fig. S6). Images of the boundary areas identify regions between the non-infiltrated and infiltrated parts of the same leaf, showing an intact structure with evidence of the homogeneously distributed particles only in infiltrated regions (Fig. 1F).

As chlorophyll concentration is not a complete measurement of plant health, we further studied the photosynthetic capability of these modified plant leaves with a portable photosynthesis system (Li-Cor) (see Materials and Methods) (37). All watercress leaves in this experiment conducted during the 12 days were infiltrated with either mSA phosphor particles (50 mg/ml) or a buffer to study the effect that infiltration alone has on plant health (fig. S7). The values of net CO<sub>2</sub> assimilation rates (A) that we measured for watercress are typical for plants with a C3 carbon fixation mechanism, which results in high assimilation values (38). By fitting the A and C<sub>i</sub>

(intercellular CO<sub>2</sub> concentration) data, we determined the  $V_{c,max}$  constant of the Rubisco-RuBP complex (39, 40). We observed that a reduction in  $V_{c,max}$  for modified plants from  $26 \pm 1$  to  $22 \pm 1$   $\mu\text{mol m}^{-2} \text{s}^{-1}$  directly after infiltration was typical for both the particle and buffer conditions. On the 12th day after infiltration,  $V_{c,max}$  was reduced to  $8.8 \pm 2.4$   $\mu\text{mol m}^{-2} \text{s}^{-1}$ , while our control plants, either five plants modified with buffer only or five plants kept intact, showed  $V_{c,max}$  values of  $7.3 \pm 2.2$  and  $4.7 \pm 2.6$   $\mu\text{mol m}^{-2} \text{s}^{-1}$ , respectively (fig. S8). This shows that modified plants keep a similar photosynthetic functionality as that of nontreated plants, enabling CO<sub>2</sub> capture under modified conditions. This sharp decrease in  $V_{c,max}$  for all samples is likely because of the plant aging effect. To support this, we studied the relationship between the chlorophyll concentration of different-aged leaves from the same plant and the corresponding CO<sub>2</sub> assimilation response on the same day. Here, the A versus C<sub>i</sub> response was measured in mature, 5-week-old plants, starting from the second oldest leaf (second from the bottom of the stem) to the youngest (at the top of the plant) (fig. S9). Both measurements show a linear relationship ( $R^2 = 0.91$ ) between chlorophyll concentration and age, from  $29 \pm 1.7$  to  $20 \pm 0.4$  SPAD, and corresponding RuBP activity (i.e.,  $V_{c,max}$ ), from  $26 \pm 6.9$  to  $8.1 \pm 3.3$   $\mu\text{mol m}^{-2} \text{s}^{-1}$ . This showed that older leaves have reduced chlorophyll concentration over time, which leads to reduced RuBP activity.

Next, we studied the size dependence of infiltrated mSA NPs. We infiltrated each sample into 3-week-old plant leaves as described with a final particle concentration of 50 mg/ml (Fig. 5). Infiltrated leaves were extensively washed with tap water to remove non-infiltrated particles from the leaf surface. Afterward, the leaf was left to dry at room temperature. Only sample S<sub>3</sub> with size  $650 \pm 290$  nm showed

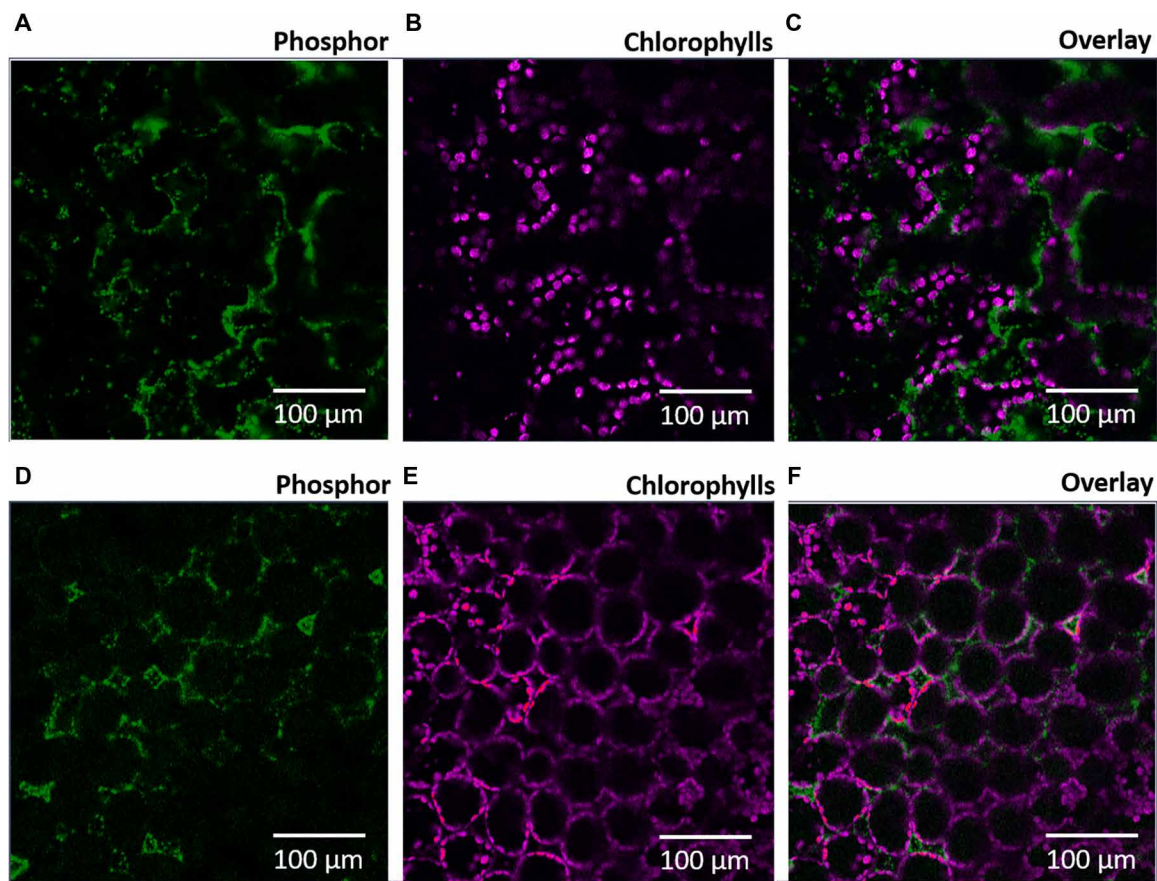


**Fig. 4. Infiltrated particle localization between mesophyll cells in modified watercress plants.** (A to C) Confocal images of infiltrated watercress with  $S_3$  mSA sample and  $S_4$  mSA sample (D to F), respectively. This supports our claim that phosphors are located within the chlorophylls.

particle penetration into the watercress stem. Sample  $S_1$  (size  $1090 \pm 400$  nm) showed heterogeneous behavior; a small portion of particles propagated along through the leaves, while larger particles remained at the infiltration points ( $S_1$  sample on Fig. 5A). This supports our earlier observation that larger particles cannot diffuse deeply into the leaf because of the limited size of the stomata and the extensive pressure required to infiltrate, which also damages the leaf. Samples  $S_4$  and  $S_5$ , with smaller particle sizes of  $440 \pm 280$  nm and  $390 \pm 180$  nm, respectively, showed efficient infiltration across the entire leaf area. However, they also had lower brightness, because they have a reduced volume-to-surface area ratio, which causes the lower activity of the particles. Each modified leaf was exposed to a LED ( $400 \text{ mW/cm}^2$ ) for 1 min with a maximum power intensity at 400 nm, and the optical density (OD) of the samples was measured in this absorption wavelength as well (fig. S10). Next, the absorbance of samples  $S_1$  to  $S_5$  and their phosphorescent emission intensity inside the watercress leaf were recorded for 1 hour on camera, where at each minute a single picture was taken under 30-s exposure as we established earlier (fig. S11) (5). The decay times, calculated over five leaves infiltrated with  $S_1$  to  $S_5$  samples, are  $0.6 \pm 0.1$ ,  $3.4 \pm 0.2$ ,  $6.1 \pm 0.3$ ,  $1.3 \pm 0.1$ , and  $1.0 \pm 0.1$  min, respectively. This shows that we might introduced a different amount of material into watercress leaves during infiltration. We measured each leaf in triplicate to show reproducibility and material stability inside the plants after multiple

exposures to 400-nm LED light (fig. S12). Next, we compared the same leaf modified with  $S_3$  particles at days 0 and 7 with decay times of  $6.1 \pm 0.3$  and  $6.6 \pm 0.3$  min, respectively (Fig. 5, B and C). The infiltrated watercress leaf showed a glowing leaf and stem after charging (Fig. 5D) with no reduction in light intensity (Fig. 5E). We determined the minimum required time for 85% phosphor charging is 5 s, where any extra excitation time had a minor effect on decay time (fig. S13). Last, our experiments suggest that short-time LED light flashing light has a minor impact on the plants; however, alone, it is not sufficient for plant growth (fig. S14).

In our next experiment, we sought to demonstrate that our strategy can be applied to several species of plants. We chose the commonly available commercial plants gerbera daisy (*B. perennis*), basil (*O. basilicum*), and a 2-month-old tobacco plant (*N. tabacum*) to infiltrate with Si/SiO<sub>2</sub>-coated mSA particles (50 mg/ml) of sample  $S_3$  (Fig. 6, A to C). We used our same infiltration method to homogeneously infiltrate the leaf surfaces with particles. The decay intensity of phosphorescence after identical charging showed a clear difference between those plant species with decay times of  $0.1 \pm 0.1$ ,  $1.8 \pm 0.1$ ,  $7.4 \pm 0.3$ , and  $14.6 \pm 0.5$  min for daisy, basil, watercress, and tobacco, respectively (Fig. 6, D and E). We observe an apparent correlation between the SA decay time and the average chlorophyll concentration of the plant post-infiltration after drying. This trade-off requires more study but may be caused by the different available surface areas of mesophyll

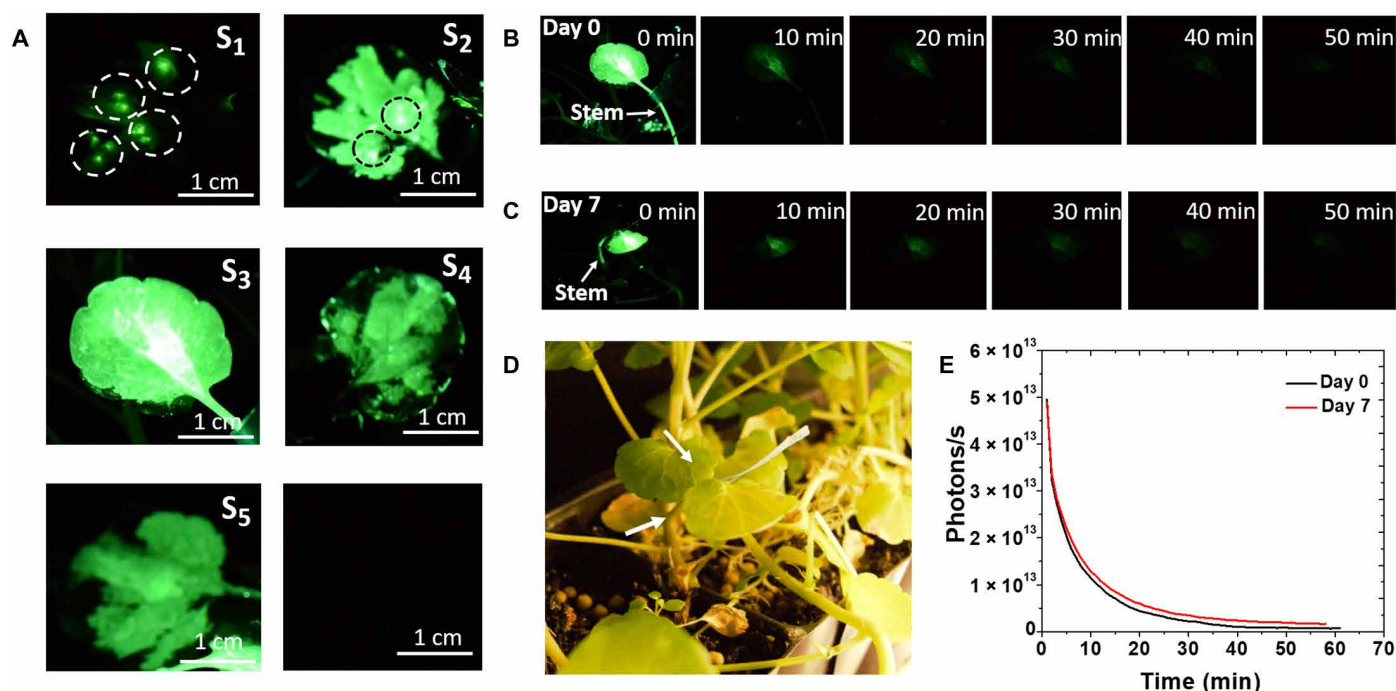


**Fig. 5. Size-dependent infiltration of mSA particles in watercress plants.** (A) Infiltrated watercress leaves with different sizes of Si/SiO<sub>2</sub>-coated mSA particles named S<sub>1</sub>, S<sub>2</sub>, S<sub>3</sub>, S<sub>4</sub>, and S<sub>5</sub> and nonmodified leaf (control). The exposure time was set at 30 s for all samples. Each leaf was charged with 400-nm LED (400 mW/cm<sup>2</sup>) for 30 s immediately before the measurements. Each measurement was continued for 1 hour. (B and C) Characteristic intensity decay pictures of glowing watercress leaf directly after infiltration (day 0) and after 1 week (day 7). (D) Optical image of the modified leaf after 1 week, where arrows indicate glowing leaf and stem. (E) Emission intensity decay profile directly after infiltration and after 1-week time frame. For the corresponding decay time in vitro and a comparison/discussion with the decay inside plant's leaves, see the Supplementary Materials. In each experiment, the emission was visible by the naked eye for 1 hour. Photo credit: Pavlo Gordiichuk, Massachusetts Institute of Technology.

phases across the species (fig. S15). This area can either inhibit or stabilize NP aggregation, which we show in this work has a strong influence on the phosphorescent lifetime (Fig. 6E).

To explore the effect of the plant mesophyll on optical properties changed by NP aggregation state, we studied this effect in vitro. We measured the decay times in solution for different concentrations of SA/SiO<sub>2</sub> NPs at the upper end of the stability range. We find that SA/SiO<sub>2</sub>-coated SA NPs aggregate, and the corresponding SA aggregates produce longer phosphorescent decay times (fig. S16). By changing the particle concentration of 1 to 50 mg/ml, we could increase the decay time from 1 to 20 min. We have developed a theoretical model (Supplementary Materials) for the explanation of this effect (fig. S17) that quantitatively links particle aggregation, even inside the plant, to decreasing decay time variations. Because of the difference in plant species, differences in surface area may lead to changing degrees of particle aggregation and, therefore, a unique emission signature in each plant species (see Materials and Methods). Overall, because of differences in plant species, the internal leaf structure can show selective permeability to a certain size ranges of particles, and as a result, we can infiltrate only below a characteristic cutoff size, which is an interesting area for further research. Overall, tobacco leaves infiltrated with mSA NPs showed an intensity decay time of close to 70% of the starting raw SA material (fig. S18).

Next, we displayed our work in a public museum exhibit at the Smithsonian Institute of Design, Manhattan, New York City, which ran for 33 weeks. In this exhibit, 3-week-old watercress plants with leaves measuring 1 to 2 cm across were infused with a nanophosphor

solution of 25 mg/ml and particle size of  $650 \pm 290$  nm. The plants were kept in a model house with self-watering and optical light tubes for illumination (fig. S19) (41). For this experimental setup, 10 plants were subjected to 10 s of LED charging with 400-nm blue light [400 mW/cm<sup>2</sup> ultraviolet (UV)-blue] followed by a display period of 5 min. We optimized our excitation strategy so that each plant was exposed to 2016 light charging/emission cycles weekly, Monday through Saturday. After each excitation cycle, the light emitted by the plants was bright enough that museum guests could view them directly or take a photo with a personal cell phone (Fig. 7A). Biweekly throughout the 33-week duration of the exhibit, 10 new plants were delivered to the museum, which resulted in over 160 light-emitting plants displayed. When the museum closed at night, we exposed plants to 9-W LED with an absolute daylight spectrum for 8 hours to allow growth and photosynthesis. After 2 weeks of the experiments, large plants transported back to the laboratory showed no observable physiological damage of the plants or brightness changes of infused nanomaterials (fig. S20). To show that light-emitting plant (LEP) emitted light could be applied for indirect illumination of sustainable buildings, in proof-of-concept experiments, we showed that glowing light amplification was possible with Fresnel lens on the distance greater than 1 m from the plant (fig. S21).

## DISCUSSION

We compared the measured light intensity produced of our plants with the chemiluminescent light of other light-emitting plant systems

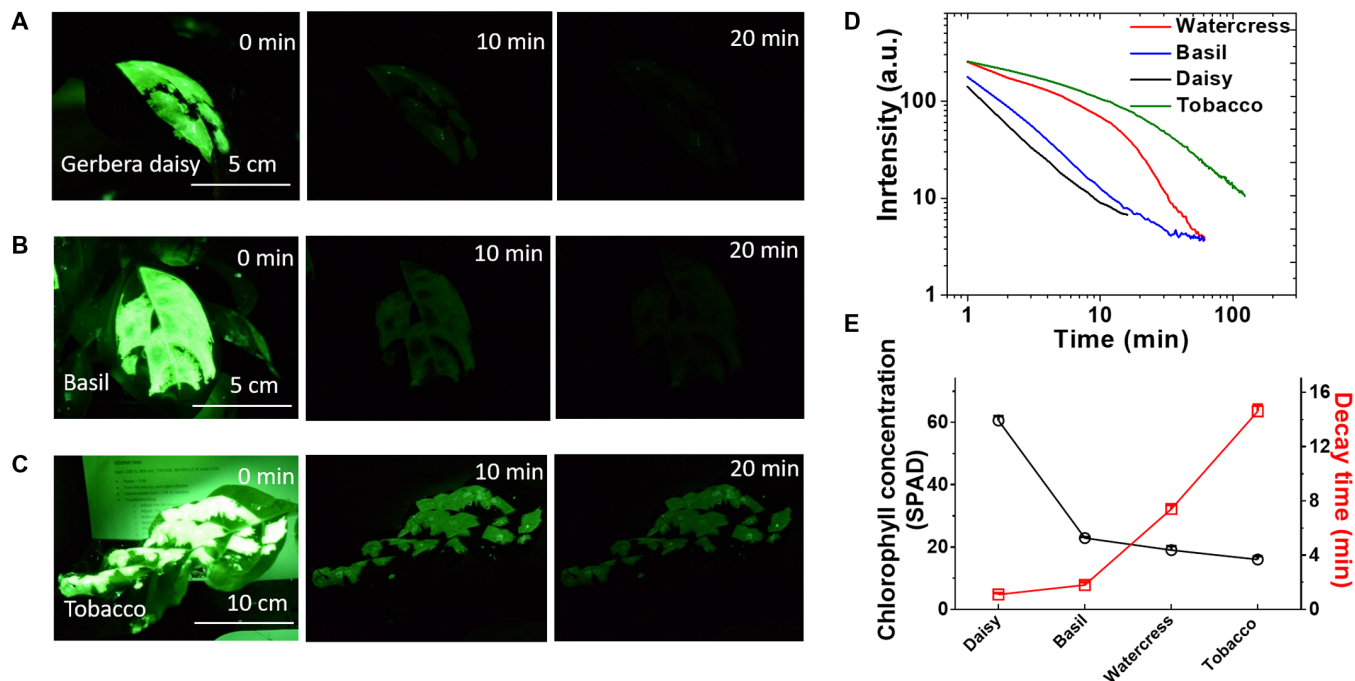


**Fig. 6. Infiltrated particle localization in commercial plants.** (A) Infiltrated gerbera daisy with  $S_3$  sample on the first week (day 0). (B) Infiltrated basil with the  $S_3$  sample on the first week (day 0). (C) Infiltrated tobacco plant with the  $S_3$  sample on the first week (day 0). (D) Log-log plot of phosphorescence intensity decay in  $1.1 \pm 0.1$ ,  $1.8 \pm 0.1$ ,  $7.4 \pm 0.3$ , and  $14.6 \pm 0.5$  min for daisy, basil, watercress, and tobacco, respectively. All measurements were performed similarly, where glowing light was recorded with a Nikon D5300, f/4.5, and ISO 6400 camera by taking a picture each minute with an exposure time of 30 s. Before the measurements, each leaf was charged with 400-nm LED (excitation fluence of  $400 \text{ mW/cm}^2$ ) for 1 hour. In each experiment, it was possible to see emission light in a dark room for 1 hour after 30-s excitation. a.u., arbitrary units. (E) The decay intensity of phosphorescence for select plant species inversely relates to the average chlorophyll concentration measured after infiltration for watercress, basil, gerbera daisy, and tobacco in SPAD units.

(Fig. 7B) (6–8).  $I_{\max}$  is the maximum observed photon intensity at the start of the measurement. Here, we define illumination lifetime as the time when the intensity falls to 90% of  $I_{\max}$  [see (10)]. The phosphorescence in this work can exceed the emission intensities of plants that generate their own emission studied in the literature. That means that the photonic capacitance demonstrated in this work could potentially augment the light generated in these other studies by, for example, being charged from or re-emitting in parallel with chemiluminescence or genetic engineering emission strategies. For this, the absorption cross section of the SA should be optimized to receive bioluminescence from the plant. This has the benefit of increasing the total amount of potential radiant light energy available for emission from the plant (i.e., augmentation with stored solar energy). In addition, the function of phosphorescent NPs as light capacitors can also smooth and regulate chemiluminescent emission to produce more even illumination [see, for example, figure 2A in (5)]. In addition, our experiments showed close to 60% SA NP recovery from the infused tobacco plants as a forcible strategy for e-waste utilization (Materials and Methods and fig. S22).

As a final proof-of-concept experiment, mSA NPs were infiltrated into 50-cm-tall seedling of a “Thailand Giant” Elephant Ear (*Colocasia*) tree. We applied mSA particles to a 30-cm-long leaf with the same infusion method as with previous plants. However, the large size of the leaf required many more point-by-point infiltrations to cover the entire area (Fig. 7C). After 10 s of charging with 400-nm blue LED ( $400 \text{ mW/cm}^2$  UV-blue), the portrait pictures were made on

Pixel 3a camera after the immediate movement of the excitation source. Because the elephant ear leaf was subjected to serial infusion, the close images recorded similarly enable illustrating of phosphor NP deposition along either side of the mid-vein along the secondary veins as shown in Fig. 7E. The recorded images showed efficient lateral spreading of the NPs along the leaf, even between veins, and demonstrated the potential scalability of our methods to large, potentially meter-sized plants.

In conclusion, we investigated the mesophyll region of living plants as a biocompatible substrate for the photonic display of thin nanophosphor films, with the ultimate goal of creating living plant optical devices. We find that size-sorted, silica-coated SA NPs can be successfully infused into the mesophyll through the stomata pores of tobacco (*N. tabacum*), basil (*O. basilicum*), daisy (*B. perennis*), watercress (*N. officinale*), and *Colocasia* (also called Thailand Giant Elephant Ear) plants. Our work demonstrates that infused SA NPs remain in the spongy mesophyll area of plant leaves without entering into the plant cells themselves. Unexpectedly, maximum phosphorescent emission intensities per plant approach  $4.8 \times 10^{13}$  photons/s, which is sufficient to advance plant-based emission strategies. Biocompatibility is examined by long-term chlorophyll concentrations measured across 180 watercress plants over a period of 9 days after infiltration. We mapped the trade-off between phosphorescent decay time and particle size for Si/SiO<sub>2</sub>-coated species, balancing infusion efficiency with desired optical properties for the first time. Our work demonstrates long-term robustness by examining a cohort of 160 plants,

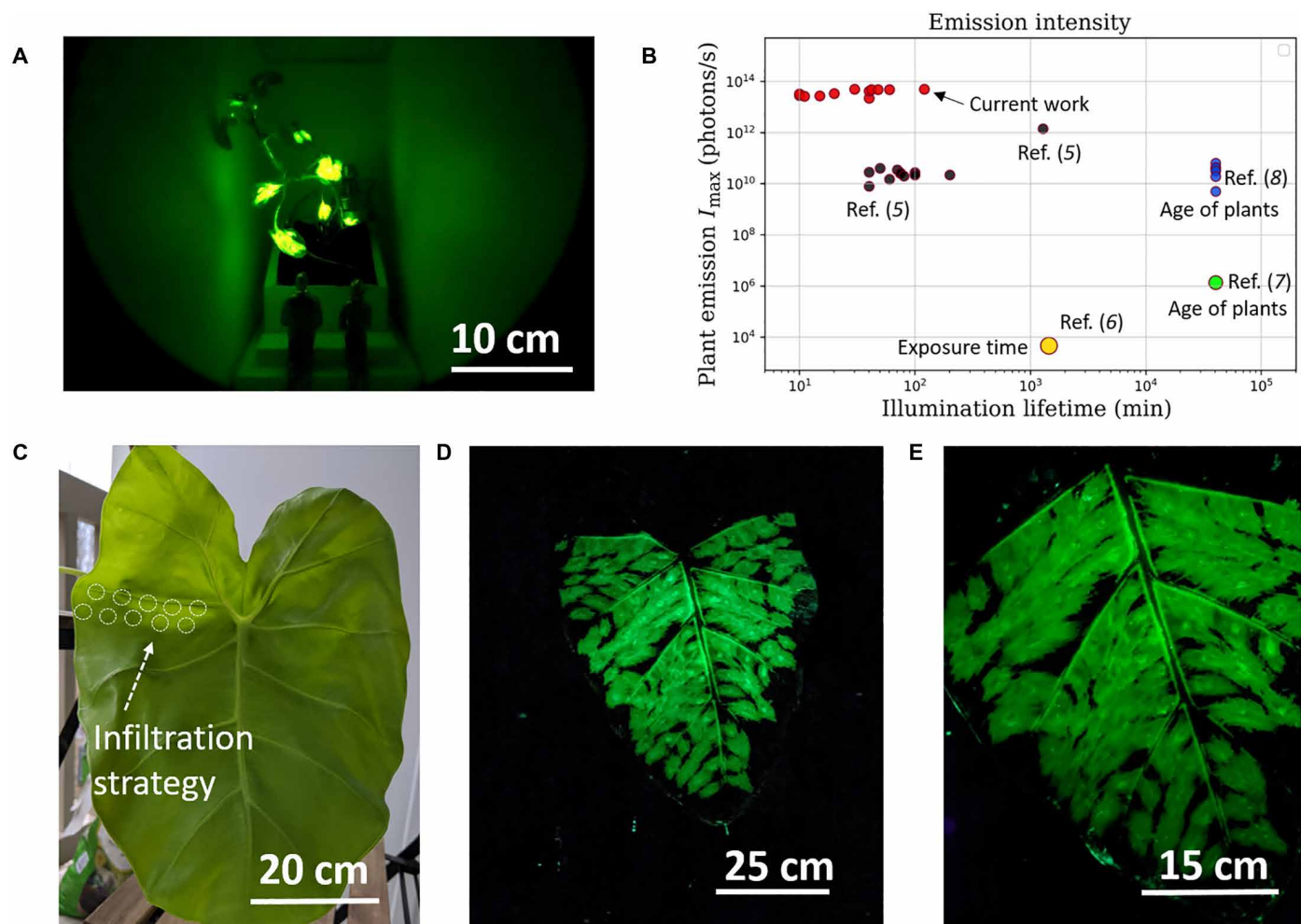


**Fig. 7. Applications of SA NPs in model plants and large trees.** (A) Three-week-old watercress plant infiltrated with  $650 \pm 290$ -nm  $\text{SiO}_2$ -coated phosphors used in an exhibit at the Smithsonian Museum of Design, New York, New York (May 2019 to January 2020). (B) Comparison plot benchmarking phosphorescent emission in plants for this work compared to chemiluminescent plants (5) and several genetically modified light-emitting plants (6–9). The comparison shows that the light capacity and phosphorescent intensities at the concentrations used in this work can potentially augment the light emission of previous efforts. (C) The elephant ear plant (*Colocasia*), 20-cm leaf subjected to serial infusion along the secondary veins as shown. (D) Resulting phosphorescence after 10-s charging at  $400 \text{ mW/cm}^2$ , portrait picture made on Pixel 3a camera after the excitation source was removed. (E) Increased magnification from illustrating phosphor deposition along either side of the mid-vein. Photo credit: Pavlo Gordiichuk, Massachusetts Institute of Technology.

which were subjected to alternating cycles of charging and emission for 16 hours a day for approximately 2 weeks without observable impact to plant physiology. Hence, our work advances the fabrication and characterization required to transform living plants into functioning photonic substrates. Therefore, this enables opportunities for plant-based optical reflectance, signaling, and the augmentation of plant-based light emission.

## MATERIALS AND METHODS

### Phosphor milling

One hundred grams of SA powder was dispersed in 100 ml of ethyl acetate in a 300-ml ceramic milling jar (U.S. Stoneware Roalox Alumina-Fortified Grinding Jar) with small and large zirconia cylinders as the grinding media in the rotation mill (Labmill-8000, 1 Tier, 115/220 V VAC) for 7 to 14 days. Afterward, the remaining ethyl acetate was removed under nitrogen gas, and dried samples were used for further modification steps.

### Si/SiO<sub>2</sub> coating of milled phosphor NPs

We have suspended 500 mg of milled SA powder in 100 ml of anhydrous ethanol in a 100-ml glass vial and sealed it with a plastic cap. Next, 25 ml of MilliQ water and 3.3 ml of tetraethyl orthosilicate were added to the solution and sonicated (Branson 2800 Sonicator) for 10 min, followed by adding 12 ml of aqueous ammonium hydroxide (28 to 30%). After, the sample was stirred for 12 hours at 300 rpm at room temperature (22°C). Adding additional water terminated the reaction followed by a 1.5-hour centrifugation step (Eppendorf 5810R at 4000 rpm), after which the particle precipitate was resuspended in fresh deionized (DI) water.

### Determination of extinction coefficient

Several mSA particle concentrations prepared by the weighting of dry powder followed within several dilutions in DI water, ranging between 0.02 and 0.3 mg/ml, were used for UV-visible absorbance measurements, and calculation of corresponding extinction coefficient at 400 nm, resulting in  $0.4 \pm 0.1 \text{ OD (mg/ml)}^{-1}$  (fig. S10).

## Sorting of Si/SiO<sub>2</sub>-coated nanophosphor

### Part 1

Freshly coated milled NPs with Si/SiO<sub>2</sub> shell (500 mg) were gently sonicated for 1 min in Branson 2800 Sonicator and spun down in centrifuge Eppendorf 5810R at 4000 rpm at different times ranging from 70 to 1 min, respectively. After each sonication step, the supernatant (containing nonmeasured sedimentation particles) was removed and concentrated with a Millipore filter with 100K molecular cutoff Amicon Ultra-15 Centrifugal Filter Units.

### Part 2

We centrifuged Si-coated poly-sized starting particles at 4000-rpm speed for 1 min, which resulted in the precipitation of larger particles. However, the remaining supernatant contained many non-sedimenting particles, which we collected and labeled as the first (S<sub>5</sub>) sample. Next, we resuspended the pellet in fresh DI water and repeated the centrifugation again for the same time at a lower rotation speed (3000 rpm), where we treated the resulting supernatant as the second (S<sub>4</sub>) sample. We repeated this procedure for 2000-, 1000-, and 500-rpm rotation speeds leading to S<sub>3</sub>, S<sub>2</sub>, and S<sub>1</sub> samples, respectively.

## Characterization of NPs

Particles milled and size-sorted by centrifugation were subjected to a  $\zeta$ -potential measurement, which was averaged over 10 runs using a phase analysis light scattering zeta potential analyzer (PALS) (Nano Brook Zeta PALS Potential Analyzer, NY, USA). We analyzed the NP sizes with NanoSight LM10 (NanoSight Ltd., Amesbury, UK) and SEM JSM-6010LA InTouch Scope (JEOL Ltd.).

## Plant growth

We performed experiments on 3- to 4-week-old watercress plants. We purchased plant seeds from David's Garden Seeds (TX, USA) and grown in a plant growth chamber (Adaptis 1000, Conviron, Canada) at fixed 60% humidity, 22°C, and 16-hour light/8-hour dark.

## Plant infiltration

Plants were infiltrated such that infused liquid could diffuse along the leaves in all directions from the infiltration point (Fig. 3A). This infiltration strategy confirmed that phosphor particles could travel inside infiltrated leaves at far distances (up to 2 cm) from the contact point. Second, modified leaves were intensively washed with DI water to ensure the removal of any remaining non-infiltrated particles from leaf surfaces. In addition, we prepared each of the five samples at several particle concentrations (1, 5, 10, 25, and 50 mg/ml) and infiltrated in five watercress plants.

## Characterization with cryo-SEM

We infiltrated a single watercress leaf with 200  $\mu$ l of a particle solution (50 mg/ml) and one with solely buffer 1 day before measurement. After we cut the leaves 1 cm below at their stems, both modified and nonmodified leaves from the same plant were instantaneously frozen and studied under the same conditions, from a top and cross-section view with SEM.

## Fluorescent confocal microscopy

Confocal images were taken with a Zeiss LSM 710 NLO microscope. The watercress leaf discs (~2 mm in radius) were prepared and placed on a microscope glass slide with a polydimethylsiloxane chamber. In addition, we filled the leaf with perfluorodecalin to increase image

resolution. Images were taken with a 40 $\times$  water immersion objective. Optical images of modified watercress leaves were taken at 620 to 700 nm (autofluorescence of chlorophylls) with 632-nm excitation and 510- to 550-nm emission (phosphorescence of mSA particles with 488-nm excitation from both S<sub>3</sub> and S<sub>4</sub> samples).

## Measurement with Li-Cor portable photosynthetic system

One plant was infiltrated with buffer, and we studied two intact watercress plants as biological references. All seven plants were measured immediately after infiltration and, subsequently, every 2 or 3 days. The net CO<sub>2</sub> assimilation rate (*A*), as a function of internal CO<sub>2</sub> concentrations (*C<sub>i</sub>*), was based on reference CO<sub>2</sub> concentrations of 1200, 1000, 800, 600, 400, 300, 200, 100, 50, and 0  $\mu$ mol mol<sup>-1</sup>, a light set point of 900  $\mu$ mol m<sup>-2</sup> s<sup>-1</sup>, relative humidity of 50%, and room temperature 25°C.

## Determination of V<sub>c,max</sub>

V<sub>c,max</sub> was calculated using Excel macros published (39). The real-time temperature was measured and included in the calculation for a more accurate prediction.

## Recovery of SA NPs from LEPs

The problem of e-waste was addressed by the secondary SA NP extraction from fabricated LEPs. Infused leaves with SA NPs were dried for 1 hour at 200°C, mechanically milled, and ultrasonicated. By applying 400-rpm centrifuging speed for 1 min, SA NP particles showed fast precipitation into a white pellet at the bottom of the 50-ml tube. The centrifuging procedure was repeated five times, where the collected samples were dried at 70°C for 12 hours and weighted, which overall resulted in 30 mg of SA white powder. This strategy helped to recover up to 60% by weight SA materials (fig. S22).

## SUPPLEMENTARY MATERIALS

Supplementary material for this article is available at <https://science.org/doi/10.1126/sciadv.abe9733>

## REFERENCES AND NOTES

1. T. T. S. Lew, V. B. Koman, P. Gordiichuk, M. Park, M. S. Strano, The emergence of plant nanobionics and living plants as technology. *Adv. Mater. Technol.* **5**, 1900657 (2019).
2. M. H. Wong, J. P. Giraldo, S. Y. Kwak, V. B. Koman, R. Sinclair, T. T. S. Lew, G. Bisker, P. Liu, M. S. Strano, Nitroaromatic detection and infrared communication from wild-type plants using plant nanobionics. *Nat. Mater.* **16**, 264–272 (2017).
3. R. Di Giacomo, C. Daraio, B. Maresca, Plant nanobionic materials with a giant temperature response mediated by pectin-Ca<sup>2+</sup>. *Proc. Natl. Acad. Sci. U.S.A.* **112**, 4541–4545 (2015).
4. E. Stavrinidou, R. Gabrielson, E. Gomez, X. Crispin, O. Nilsson, D. T. Simon, M. Berggren, Electronic plants. *Sci. Adv.* **1**, e1501136 (2015).
5. S. Y. Kwak, J. P. Giraldo, M. H. Wong, V. B. Koman, T. T. S. Lew, J. Ell, M. C. Weidman, R. M. Sinclair, M. P. Landry, W. A. Tisdale, M. S. Strano, A nanobionic light-emitting plant. *Nano Lett.* **17**, 7951–7961 (2017).
6. D. W. Ow, J. R. DE Wet, D. R. Helinski, S. H. Howell, K. V. Wood, M. Deluca, Transient and stable expression of the firefly luciferase gene in plant cells and transgenic plants. *Science* **234**, 856–859 (1986).
7. A. Krichevsky, B. Meyers, A. Vainstein, P. Maliga, V. Citovsky, Autoluminescent plants. *PLOS ONE* **5**, e15461 (2010).
8. T. Mitiouchkina, A. S. Mishin, L. G. Somermeyer, N. M. Markina, T. V. Chepurnyh, E. B. Guglya, T. A. Karataeva, K. A. Palkina, E. S. Shakhova, L. I. Fakhranurova, S. V. Chekova, A. S. Tsarkova, Y. V. Golubev, V. V. Negrebetsky, S. A. Dolgushin, P. V. Shalaev, D. Shlykov, O. A. Melnik, V. O. Shipunova, S. M. Deyev, A. I. Bubyrev, A. S. Pushin, V. V. Choob, S. O. Dolgov, F. A. Kondrashov, I. V. Yampolsky, K. S. Sarkisyan, Plants with genetically encoded autoluminescence. *Nat. Biotechnol.* **38**, 944–946 (2020).
9. J. P. Giraldo, M. P. Landry, S. M. Faltermeier, T. P. McNicholas, N. M. Iverson, A. A. Boghossian, N. F. Reuel, A. J. Hilmer, F. Sen, J. A. Brew, M. S. Strano, Plant nanobionics approach to augment photosynthesis and biochemical sensing. *Nat. Mater.* **13**, 400–408 (2014).

10. J. P. Giraldo, H. H. Wu, G. M. Newkirk, S. Kruss, Nanobiotechnology approaches for engineering smart plant sensors. *Nat. Nanotechnol.* **14**, 541–553 (2019).
11. T. T. S. Lew, V. B. Koman, K. S. Silmore, J. S. Seo, P. Gordiichuk, S. Y. Kwak, M. Park, M. C. Y. Ang, D. T. Khong, M. A. Lee, M. B. Chan-Park, N. H. Chua, M. S. Strano, Real-time detection of wound-induced H<sub>2</sub>O<sub>2</sub> signalling waves in plants with optical nanosensors. *Nat. Plants* **6**, 404–415 (2020).
12. R. E. Blankenship, *Molecular Mechanisms of Photosynthesis* (Blackwell Science Ltd., 2008).
13. J. M. Nassar, S. M. Khan, D. R. Villalva, M. M. Nour, A. S. Almuslem, M. M. Hussain, Compliant plant wearables for localized microclimate and plant growth monitoring. *npi Flex. Electron.* **2**, 24 (2018).
14. Y. Zhao, S. Gao, J. Zhu, J. Li, H. Xu, K. Xu, H. Cheng, X. Huang, Multifunctional stretchable sensors for continuous monitoring of long-term leaf physiology and microclimate. *ACS Omega* **4**, 9522–9530 (2019).
15. W. Tang, T. Yan, J. Ping, J. Wu, Y. Ying, Rapid fabrication of flexible and stretchable strain sensor by chitosan-based water ink for plants growth monitoring. *Adv. Mater.* **2**, 1700021 (2017).
16. V. B. Koman, T. T. S. Lew, M. H. Wong, S. Y. Kwak, J. P. Giraldo, M. S. Strano, Persistent drought monitoring using a microfluidic-printed electro-mechanical sensor of stomata in planta. *Lab Chip* **17**, 4015–4024 (2017).
17. M. M. Damak, S. R. Mahmoudi, M. D. Hyder, K. K. Varanasi, Enhancing droplet deposition through in-situ precipitation. *Nat. Commun.* **7**, 12560 (2018).
18. S. Y. Kwak, T. T. S. Lew, C. J. Sweeney, V. B. Koman, M. H. Wong, K. Bohmert-Tatarev, K. D. Snell, J. S. Seo, N. H. Chua, M. S. Strano, Chloroplast-selective gene delivery and expression in planta using chitosan-complexed single-walled carbon nanotube carriers. *Nat. Nanotechnol.* **14**, 447–455 (2019).
19. G. S. Demireh, H. Zhang, J. L. Matos, N. S. Goh, F. J. Cunningham, Y. Sung, R. Chang, A. J. Aditham, L. Chio, M. J. Cho, B. Staskawicz, M. P. Landry, High aspect ratio nanomaterials enable delivery of functional genetic material without DNA integration in mature plants. *Nat. Nanotechnol.* **14**, 456–464 (2019).
20. T. T. S. Lew, M. H. Wong, S.-Y. Kwak, R. Sinclair, V. B. Koman, M. S. Strano, Rational design principles for the transport and subcellular distribution of nanomaterials into plant protoplasts. *Small* **14**, e1802086 (2018).
21. M. H. Wong, R. P. Misra, J. P. Giraldo, S. Y. Kwak, Y. Son, M. P. Landry, J. W. Swan, D. Blankschtein, M. S. Strano, Lipid exchange envelope penetration (LEEP) of nanoparticles for plant engineering: A universal localization mechanism. *Nano Lett.* **16**, 1161–1172 (2016).
22. Y. Yu, J. Wang, Y. N. Zhu, M. Q. Ge, Researches on preparation and properties of polypropylene nonwovens containing rare earth luminous materials. *J. Rare Earths* **32**, 1196–1200 (2014).
23. Y. T. Guo, Y. M. Huang, Green aluminate phosphors used for information display. *Key Eng. Mater.* **428-429**, 421–425 (2010).
24. B. C. Jamalajah, Y. R. Babu, Near UV excited SrAl<sub>2</sub>O<sub>4</sub>:Dy<sup>3+</sup> phosphors for white LED applications. *Mater. Chem. Phys.* **211**, 181–191 (2018).
25. K. Van den Eeckhout, D. Poelman, P. F. Smet, Persistent luminescence in Non-Eu<sup>2+</sup>-doped compounds: A review. *Materials* **6**, 2789–2818 (2013).
26. Y. Li, M. Gecevicius, J. R. Qiu, Long persistent phosphors—from fundamentals to applications. *Chem. Soc. Rev.* **45**, 2090–2136 (2016).
27. Y. R. Do, J. W. Bae, Application of photoluminescence phosphors to a phosphor-liquid crystal display. *J. Appl. Phys.* **88**, 4660–4665 (2000).
28. H. Takasaki, S. Tanabe, T. Hanada, Long-lasting afterglow characteristics of Eu, Dy codoped SrO-Al<sub>2</sub>O<sub>3</sub> phosphor. *J. Ceram. Soc. Jpn.* **104**, 322–326 (1996).
29. T. Matsuzawa, Y. Aoki, N. Takeuchi, Y. Murayama, New long phosphorescent phosphor with high brightness, SrAl<sub>2</sub>O<sub>4</sub>:Eu<sup>2+</sup>, Dy<sup>3+</sup>. *J. Electrochem. Soc.* **143**, 2670–2673 (1996).
30. C. H. Lu, S. Y. Chen, C. H. Hsu, Nanosized strontium aluminate phosphors prepared via a reverse microemulsion route. *Mater. Sci. Eng. B Solid* **140**, 218–221 (2007).
31. J. Geng, Z. Wu, Synthesis of long afterglow SrAl<sub>2</sub>O<sub>4</sub>:Eu<sup>2+</sup>, Dy<sup>3+</sup> phosphors through microwave route. *J. Mater. Synth. Process.* **10**, 245–248 (2002).
32. Z. L. Tang, F. Zhang, Z. T. Zhang, C. Y. Huang, Y. H. Lin, Luminescent properties of SrAl<sub>2</sub>O<sub>4</sub>:Eu,Dy material prepared by the gel method. *J. Eur. Ceram. Soc.* **20**, 2129–2132 (2000).
33. S. Y. Kaya, E. Karacaoglu, B. Karasu, Particle size influence of starting batches on phosphorescence behaviour of Sr<sub>4</sub>Al<sub>14</sub>O<sub>25</sub> based bluish green phosphors. *Adv. Appl. Ceram.* **111**, 393–397 (2012).
34. T. W. H. N. Luitel, T. Torikai, M. Yada, Effects of particle size and type of alumina on the morphology and photoluminescence properties of Sr<sub>4</sub>Al<sub>14</sub>O<sub>25</sub>:Eu<sup>2+</sup>/Dy<sup>3+</sup> phosphor. *Res. Lett. Mater. Sci.* **2009**, 475074 (2009).
35. D. Xiong, J. Chen, T. Yu, W. Gao, X. Ling, Y. Li, S. Peng, J. Huang, SPAD-based leaf nitrogen estimation is impacted by environmental factors and crop leaf characteristics. *Sci. Rep.* **5**, 13389 (2015).
36. G. Krouk, S. Ruffel, R. A. Gutiérrez, A. Gojón, N. M. Crawford, G. M. Coruzzi, B. Lacombe, A framework integrating plant growth with hormones and nutrients. *Trends Plant Sci.* **16**, 178–182 (2011).
37. Q. Song, X. G. Zhu, Measuring canopy gas exchange using canopy photosynthesis and transpiration systems (CAPTS). *Methods Mol. Biol.* **1770**, 69–81 (2018).
38. J. R. Evans, Photosynthesis and nitrogen relationships in leaves of C-3 plants. *Oecologia* **78**, 9–19 (1989).
39. C. J. Bernacchi, E. L. Singsaas, C. Pimentel, A. R. Portis, S. P. Long, Improved temperature response functions for models of Rubisco-limited photosynthesis. *Plant Cell Environ.* **24**, 253–259 (2001).
40. R. E. Mcmurtrie, Y. P. Wang, Mathematical models of the photosynthetic response of tree stands to rising CO<sub>2</sub> concentrations and temperatures. *Plant Cell Environ.* **16**, 1–13 (1993).
41. <https://srg.mit.edu/lep/>, <https://bosefellows.mit.edu/projects/light-emitting-plants/>.

**Acknowledgments:** We thank the Nanotechnology Materials Lab and the Koch Institute for Integrative Cancer Research, MIT, for cryo-SEM measurements. **Funding:** This research was supported by Thailand Magnolia Quality Development Corporation Limited (MQDC) (grant #6939906) and Amar G. Bose Research Grant (#2116602). S.C. was supported by MIT's Advanced Undergraduate Research Opportunities Program (Super-UROP). T.T.S.L. was supported on a graduate fellowship by the Agency of Science, Research and Technology, Singapore. M.P. was supported by the Samsung scholarship. M.K. acknowledges support by the German Research Foundation (DFG) Research Fellowship KU 3952/1-1. **Author contributions:** P.G. and M.S.S. designed experiments. P.G. performed SA fabrication and analysis and conducted experiments in plants. S.C. performed particle size analysis and conducted Li-Cor measurements and analysis. G.Z. and M.S.S. developed two theoretical models. T.T.S.L., J.C., A.M.B., M.K., and M.P. helped with particle ζ-potential measurements, particle sorting, and data interpretation. K.H., A.M.G., D.J.M.M., Z.K., and S.K. designed model house and provided Fig. 7A and fig. S19 (A to C) images. G.Z. and M.S.S. helped to model experiments. P.G. and M.S.S. wrote the manuscript. **Competing interests:** M.S.S. and P.G. are inventors on a pending patent filed by the Massachusetts Institute of Technology (no. US20200347392A1, filed on 5 November 2020). M.S.S. is an inventor on a pending patent filed by the Massachusetts Institute of Technology (no. US20180317415A1, filed on 8 November 2018). The authors declare no other competing interests. **Data and materials availability:** All data needed to evaluate the conclusions in the paper are present in the paper and/or the Supplementary Materials.

Submitted 25 September 2020

Accepted 20 July 2021

Published 8 September 2021

10.1126/sciadv.abe9733

**Citation:** P. Gordiichuk, S. Coleman, G. Zhang, M. Kuehne, T. T. S. Lew, M. Park, J. Cui, A. M. Brooks, K. Hudson, A. M. Graziano, D. J. M. Marshall, Z. Karsan, S. Kennedy, M. S. Strano, Augmenting the living plant mesophyll into a photonic capacitor. *Sci. Adv.* **7**, eabe9733 (2021).